Real-time defect detection through lateral monitoring of secondary process emissions during ultrashort pulse laser microstructuring

Milena Zuric* and Andreas Brenner
Fraunhofer Institute for Laser Technology ILT, Aachen, Germany

Abstract. Ultrashort pulse (USP) laser machining is characterized both by high spatial precisions as well as rapid changes during the processing. Laser pulses with durations of only a few hundred femtoseconds are deflected over the workpiece surfaces at speeds of up to 10 m/s. Due to the tradeoff between the precision and the productivity, USP laser machining processes can last up to multiple days. Online defect detection and their elimination is therefore essential in order to increase the stability of the established processing as well as accelerate the process development. However, monitoring of USP laser micromachining represents a great challenge because of both the high requirements for the spatial accuracy and the cost-intensive sensor integration. In the scope of this work, this challenge is tackled by laterally collecting the optical process emissions with photodiodes for different wavelength ranges. The monitoring system, which had previously been developed and had undergone initial testing, is further evaluated in this work. These most recent analyses aim to investigate the detection of the surface roughness prior to as well as its evolution during the USP laser machining. In addition, successful localization of defects induced on the workpiece surface by the USP processing is shown. Furthermore, the possibility of online process control was demonstrated by transferring the analysis algorithms to a field programmable gate array (FPGA) and implementing a real-time defect detection and feedback to the user. A decision for each data point is generated within the 10-μs cycle of the data acquisition. Furthermore, the system can be programmed flexibly and thus expanded to include real-time data analyses for further applications as well as process control. In conclusion, the analyses of laterally recorded secondary emissions have shown great potential for differentiating between surface roughness above 1 μm as well as tracking changes for every pass over the surface and localizing defects during the USP-laser machining. © *The Authors. Published by SPIE under a Creative Commons Attribution 4.0 International License. Distribution or reproduction of this work in whole or in part requires full attribution of the original publication, including its DOI.* [DOI: 10.1117/1.OE.61.9.094101]

Keywords: online monitoring; ultrashort pulse; surface structuring; real-time defect detection; process control; secondary emissions; photodiodes.

Paper 20220162G received Feb. 18, 2022; accepted for publication Aug. 22, 2022; published online Sep. 8, 2022.

1 Introduction

By means of the ultrashort pulse (USP) laser processing, surfaces of a wide variety of materials can be manipulated with micrometer precision and a negligible thermal load. Metals can therefore be structured almost melt-free, allowing USP laser processing to address numerous applications in many industrial sectors. The diversity of applications as well as processable materials and alloys continuously require new process development. However, this development is highly time-consuming due to the complexity of the USP laser processing itself. In addition, even the industrial grade machining often takes a long time. A prominent example is the several of days lasting manufacturing of steel tools for car dashboard molding. The resulting need for detection and elimination of any instabilities as early as possible increases the importance of monitoring of surface properties in parallel to the machining. However, the constant requirement for more efficiency leads to a further acceleration of the processing. This in turn complicates the online

*Address all correspondence to Milena Zuric, milena.zuric@ilt.fraunhofer.de

monitoring as it requires an increase in sampling rates with simultaneously maintaining a high spatial resolution.

Nevertheless, different systems for online quality monitoring of laser-based processing have been under development for many decades. For traditional laser applications, various approaches have already been presented in scientific publications. Some of them have even been implemented in the industrial environment.[1–3] Among the different features and phenomena, the secondary process emissions—acoustic, infrared (IR), and visible (VIS) emissions—as well as the back reflection of the processing laser have all been investigated.[4] However, the potential of process monitoring in laser welding are far from exhausted. The newest publications describe advanced sensor technologies and innovative data analysis concepts. An example of the former is the detection of airborne and structure-borne sound at up to 1 MHz.[5] Newest analysis concepts are predominantly characterized by the usage of machine learning algorithms, e.g., on camera images.[6] Beside welding, there are plenty of publications in the fields of monitoring the laser beam cutting,[7,8] as well as additive manufacturing.[9–11]

Compared with the conventional laser-based processes, the literature on process monitoring of USP laser micromachining is still scarce. When available, it describes highly restricted cases. An obvious example is the detection of the breakthrough moment during drilling. For this purpose, both coaxial and lateral detection of different optical emissions with different drilling techniques have proven to be suitable. [12,13] Further approaches describe a direct online depth measurement, e.g., interferometry,[14] shock wave detection via piezoelectric detectors,[15] and investigation of plasma generated by the process.[16] Multisensor approaches have been reported as well, such as the simultaneous monitoring of acoustic and optical emissions.[17]

In comparison to laser drilling, online quality monitoring of USP laser structuring represents a greater challenge since the aspect ratios are much lower and no breakthrough occurs. Nevertheless, descriptions of different concepts for online monitoring of the USP surface structuring are present in the scientific literature as well.

For example, a simple approach for collecting acoustic emissions has been reported to successfully detect changes in the focus position and laser power. This was achieved by analyzing the amplitude of the acoustic signal at the laser pulse repetition rate.[18] Furthermore, similar analyses of acoustic process emissions had already been carried out near the end of the last century for theoretical studies of USP laser ablation[19,20] and evaluated for determining the ablation rate.[21] However, the repetition rates used in this work were two to three orders of magnitude lower than those commonly used today.

To similarly monitor processes with higher repetition rates, microphones with frequency ranges of up to at least several hundred kilohertz are necessary, e.g., the optical microphones: they have indeed already been employed to study USP laser ablation.[22,23] However, collecting high-frequency acoustic emissions in air has a major disadvantage: the signal amplitude is strongly attenuated with the increasing frequency. Accordingly, it is necessary to mount the detector at only a few millimeters distance from the processing zone, in order to record the high-frequency components of the acoustic signal. This makes a production-oriented machine integration impossible.

There is also a possibility of recording the high-frequency acoustic signals directly on the workpiece surface.[24] Though this method poses a great challenge for the data analysis, the authors report a successful detection of the focus position by employing pattern recognition algorithms. However, an unsolvable problem here is the required mounting of the detector directly on the workpiece, making this approach unsuitable for the production environment as well.

In comparison to the acoustic emissions, the optical secondary emissions can be recorded much more easily. With a photodiode integrated with the beam path, e.g., parameters such as the focus position, the laser power, and the amount of ablated volume can be detected. Even a possibility to detect the resulting surface roughness has been suggested.[25] However, an automatic quality monitoring based on these results has not been implemented yet. Moreover, this work focuses on producing only simple wells on the workpiece surface and has not been applied to the more complex 2D structures.

Another use for a VIS-emissions-based detection is the tracking of the line width during the machining.[26] However, the results of this investigation were limited to the detection of simple features in simple geometries and their sole dependence on laser power.

For the special case of multimaterial ablation, different approaches to detect the transition to the next material have been presented. One example is camera-based and employs neural networks for the data analysis.[27] The goal of this investigation was to detect the given shape during the removal of the top material through a stencil. For a more general case, the transition to the next material is detectable using the laser-induced plasma spectroscopy.[28,29] This method is however too slow to achieve a sufficient special resolution if paired with scanner coordinates.

A further example of the AI- and camera-based quality control in laser ablation aimed to create a database of parameters and corresponding quality results for an automated support system for process developers.[30] The monitoring system was used as a reference to accelerate the investigation of the resulting quality. Due to the choice of the detector, the spatial resolution is highly limited.

Finally, there are various approaches that use the direct distance measurement to measure the quality characteristics of surfaces during the machining. One example of a measurement system integrated into the beam path is based on the ultra-high-resolution spectral domain optical coherence tomography (UHR–SD–OCT).[31] This system enables the measurement of topographies of small surface areas (up to $300 \times 300\ \mu m^2$) with an axial resolution of almost 120 nm and a lateral resolution of $<2.5\ \mu m$. However, the system is unsuitable for the real-time roughness detection because its maximum measurement frequency reaches only 1.4 kHz.

Another principle based on distance measurement for the analysis of laser structured surfaces uses the frequency domain optical coherence tomography (FD–OCT) and has an axial accuracy below one micrometer at a measurement frequency of 2 kHz.[32] Therefore, the lateral resolution of an online measurement is too low when machining is performed at typical scanning speeds. This method is however suitable for two special cases: an offline roughness measurement either before or after structuring and an online depth measurement of structures with a sufficiently large flat surface, e.g., cavities.[33]

Further successful applications of a coaxially integrated OCT system include the online distance control, ensuring the constant focus position.[34]

Although various approaches for process monitoring in USP laser micromachining have been investigated, none of them have been able to reliably and without limitations detect or predict the quality of the resulting structure yet. A tradeoff is present between the direct 3D topography measurement with low sampling rates and the faster detection of phenomena from the machining zone, requiring a more complex data analysis.

In this paper, a previously developed concept[35] for process monitoring of USP laser microstructuring is further evaluated. The monitoring is based on a lateral acquisition of optical process emissions in three wavelength ranges. The innovations described in this work include finding characteristics of these sensor data that indicate the surface condition as well as detecting the emergence of defects during the processing. The performed analyses are divided into three objectives. The first one, measuring the initial condition of the workpiece surface, is presented in Sec. 3.2. In Sec. 3.3, potentials for monitoring changes in the surface condition during machining are described, and the online detection and localization of defects are given in Sec. 4.

2 Description of the Monitoring System

2.1 *Process Monitoring Hardware*

For each of the three types of optical signals, a photodiode for the corresponding wavelength range is employed. A Si pin photodiode from Hamamatsu (S1223 01) with a sensitivity range between 350 and 1100 nm is used to detect optical emissions in the visible wavelength range. It is protected from the laser radiation by a short pass filter with a cut-off wavelength of 750 nm. Two photodiodes of the same type, G12181 010K from Hamamatsu, with a spectral sensitivity range between 950 and 1850 nm are used for detecting both the laser reflection and the infrared emission. The employed protective filters are a 1064-nm bandpass and a long pass filter with a cut-off wavelength of 1100 nm, for the laser reflection and the IR emission,

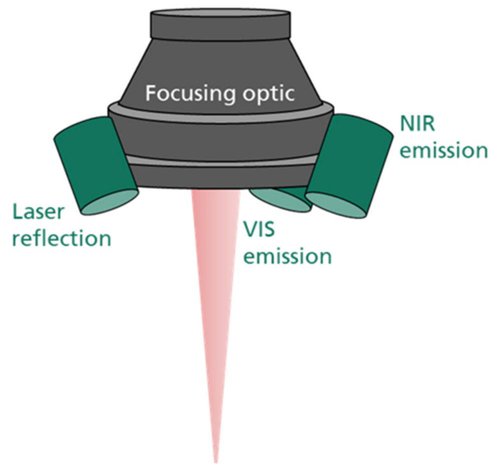

Fig. 1 Schematic representation of the detectors mounted around the focusing optic.

respectively. Additional lenses with focal lengths of 30 mm direct the light toward the corresponding detectors.

The electronic preamplification of the photodiode signals is performed with a logarithmic amplifier. The integration of the sensor system was carried out on a LASER P 1000 U machine from AgieCharmilles. The machine features a femtosecond laser from Edgewave (FX200 1 GF) with a pulse duration of 800 fs and a maximum average power of 75 W. An f-Theta lens is used as the focusing optic. The lens has a focal length of 125 mm, which leads to a spot size of 29 μm. For the beam deflection, a Scanlab galvanometer scanner intelliSCAN III 14 is used. The sensors are integrated around the f-Theta lens, as shown in Fig. 1.

To ensure repeatability of the monitoring, a holder for the sensors was designed to be mounted on the fixed housing of the optic. Therefore, the detectors are always at an exact same height above the surface of the workpiece and aligned with the center of the workpiece. Moreover, special attention was paid to the reproducibility of the position of the sensors during assembly and disassembly. The sensors are each mounted in an extended cylindrical enclosure with four screws each. Therefore, the inclination around their longitudinal axis is suppressed so that the same angle relative to the surface is always maintained, ensuring the alignment with the center of the processing field even after the sensor system had been dismantled.

2.2 *Signal Acquisition Hardware*

The signal acquisition and analysis are based on the UltraZed SOM board from Avnet. This is a hybrid system that consists of two subsystems: a field programmable gate array (FPGA) and a soft processor, combining advantages from both worlds in one chip. Among other things, the deterministic real-time capability of the FPGA is essential for this work and the processor enables a flexible implementation of the network communication, e.g., to a personal computer. The FPGA is sufficiently large to implement the needed data acquisition as well as many additional real-time analyses. The UltraZed SOM board also includes memory devices and interfaces necessary for the data acquisition and forwarding to a personal computer or a database. The 2 GB large main memory allows buffering of the sensor data for nearly 10 min. The UltraZed card is extended by a custom-made carrier board to implement the hardware connectors for communication with the laser source, scanner, machine control, and sensors.

For the analog to digital (A/D) conversion, boards based on an LTC2351 14 chip that can sample 12 analog channels at up to 250 kHz simultaneously with a resolution of 14 bits are used. To minimize the noise immunity, all digital signals are transmitted differentially between the carrier card and the A/D converter board. The information about the processing position is read directly at the communication line between the scanner and its controller at the sampling rate of 100 kHz.

3 Sensor Data Analysis

3.1 *Data Pool Creation – Machining Trials*

The purpose of the conducted experiment was to enable a comprehensive search for correlations between the recorded secondary optical emissions and the properties of the workpiece surface. This is a general investigation of the possibilities of the monitoring system, with the aim to show that the information about the surface state is contained in the collected data. In consequence, the defect-localization method developed and described in Sec. 4 is then applicable to any use case solely by tuning the analysis parameters.

Unfortunately, the intensities of the optical emissions are not decoupled from the changes in processing parameters. Furthermore, just like the processing result, the collected optical emissions are influenced by fluctuations of the laser characteristics. However, more detailed analyses of these dependencies will not be performed within the scope of this investigation since they had already been carried out and thoroughly described previously.[35] During both the experiment design and the data analysis, it is, therefore, essential to differentiate between the changes in the recorded signals caused by the processing parameters from the ones that originate from the surface. An analysis of an ill-designed data set potentially leads to a false conclusion, e.g., a detection of changing surface roughness induced solely by increasing the laser power. The rise in laser power would lead to an increase in the secondary emissions intensity. However, this does not mean that they result from the higher surface roughness, although the correlation would be present in many cases.

For this reason, during the machining trials described in this work, both the starting conditions and the processing parameters were varied. Overall, 99 different parameter combinations were used yielding areas with many different surface roughness on tool steel surfaces. The same experiment was repeated on a total of 28 specimens. They were obtained pretreated in 14 variations of machining processes, all of them being repeated twice in the sample set. The pretreatment processes include milling (23, 18, and 12 μm), polishing (0.2, 0.1, 0.05, and 0.025 μm), electrical discharge machining (6.3, 3.2, 1.6, 1.0, 0.8, and 0.4 μm), and grinding (0.6 μm). The USP-laser machining took place at constant feed rate of 3.5 m/s and constant pulse overlap of 76%. The number of pulses per burst (PPB) was varied between 1 and 10 and the single pulse peak fluence between 0.25 and 4 $\mathrm{J/cm^2}$. The repetition frequency was kept constant at 500 kHz. The number of structured layers was set for each structured area individually, in order to reach the same depth for every structure.

The data acquired during these trials was used to fulfill two of the objectives defined in the previous section. Every of the 99 first layers over each of the differently pretreated samples was analyzed in order to investigate the potential of measuring the initial surface condition. The much larger spectrum of the resulting surface roughness, due to combining the parameter and initial surface variations, was used to investigate the detection of changes during the machining.

3.2 *Detection of the Initial Surface Roughness*

To directly compare the data of the detected optical emissions with the roughness values, different characteristics were extracted from each of the time series acquired during the machining of every first structured layer. They were calculated for each sensor individually from the recorded emission intensities during the processing of the entire layer and only within the laser-on-times. To compensate for the logarithmic amplifier, prior to computing the characteristics, the raw data was linearized using exponential functions with experimentally determined factors. Therefore, the parts of the time series collected during the jumps as well as the acceleration and deceleration phases of the scanner were not taken into account.

The following approach is motivated by the assumption that the intensity of the emissions recorded by detectors at a fixed position is directly influenced by the fact that the light scatters more diffusely from rougher surfaces. For this reason, the variation of the raw data within the whole first textured layer was closely examined. To additionally achieve the independence from the processing parameters, the relative standard deviation was calculated using the equation

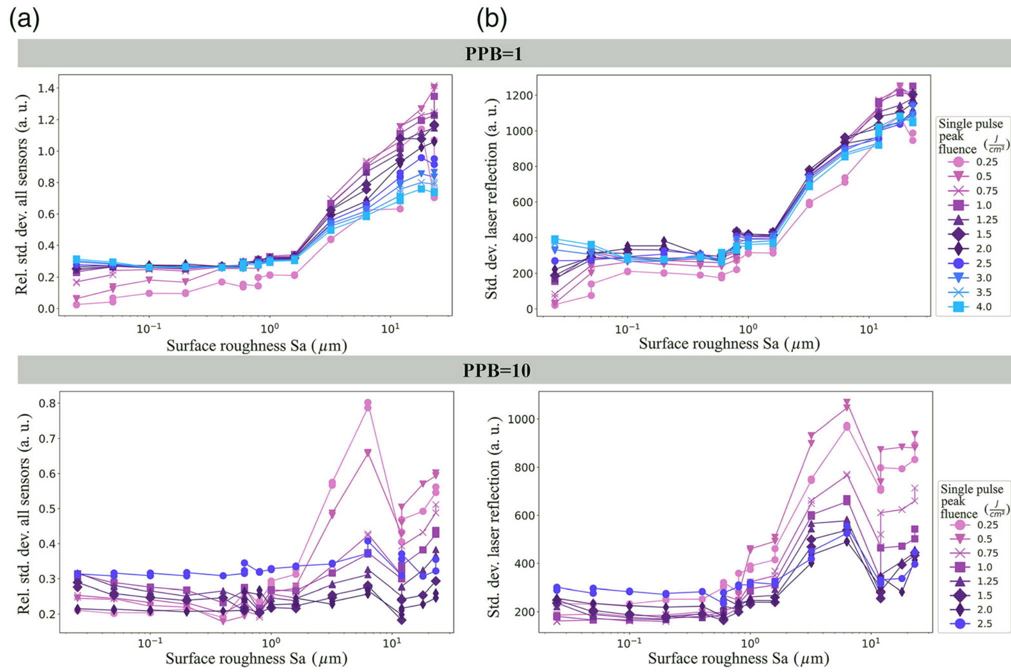

Fig. 2 (a) Relative and (b) absolute standard deviations of the sensor data during the machining of the first layers over surfaces with varying initial roughness and for changing fluences and for PPB = 1 (top graphs) and PPB = 10 (bottom graphs).

$$\sigma_{\text{rel}} = \frac{\sqrt{\frac{1}{N}\sum_{i=1}^{N}\left(\mathbf{I_i} - \frac{1}{N}\sum_{k=1}^{N}\mathbf{I_k}\right)^2}}{\frac{1}{N}\sum_{i=1}^{N}\mathbf{I_i}}, \tag{1}$$

where N is the number of datapoints in the time series and $\mathbf{I}$ the unprocessed signal intensity coming from the 14-bit A/D converters. $\mathbf{I}$ is, therefore, a unitless number between 0 and 2.[14]

Figure 2 shows the in this way extracted relative standard deviation of the secondary process emissions over the initial surface roughness for all the specimens. In all four graphs, the multiplication of previously individually calculated characteristics of all three sensors for PPB = 1 and PPB = 10 is shown.

As expected, the relative standard deviation is dependent on the surface condition. Despite its clearly visible correlation with the initial surface roughness, this feature also apparently depends on both varied processing parameters. Furthermore, even with parameters known in advance, the roughness is not clearly identifiable. While the surfaces can be differentiated from each other at a constant one pulse per burst with a known single pulse peak fluence below $F_0 = 1\ \text{J/cm}^2$, this is no longer the case at 10 pulses per burst, especially at higher fluences.

In contrast to the relative, the absolute standard deviation of the back reflection, shown on the right-hand side of Fig. 2, makes the original state detection possible for all but the three roughest surfaces preprocessed by milling. Nevertheless, the relative standard deviation is still more relevant for differentiating among the three milled surfaces. However, especially for PPB = 10, none of the features enable the distinguishing of the milled surfaces from the rest. In addition, regardless of the parameters, it is also impossible to detect the subtle differences, especially at higher laser powers. An example of this is well presented by the data of PPB = 1 and $F_0 = 4\ \text{J/cm}^2$ shown in blue.

In conclusion, considering the relative standard deviation alone is insufficient for a parameter-independent detection of the surface condition. However, a differentiation between largely different roughness regions is in most cases possible when the processing parameters are known in advance.

Due to the less promising results, the other extracted features will not be discussed separately. It is nevertheless worth mentioning that the maxima of all-optical emissions also showed a

dependence on the initial surface roughness, which would be efficient to implement in an online analysis. In contrast, and as expected, the mean intensities for all three sensors were strongly dependent on the laser fluence only. Furthermore, none of the other characteristics of the individual emissions has shown such a pronounced correlation with the surface roughness as the standard deviation of the back reflection.

3.3 *Monitoring of Changes during the Machining*

The goal of this investigation was to examine how effectively the surface roughness that results from the USP processing can be detected from the secondary emissions. Therefore, analogously to the previous section, various characteristics of the detected secondary emissions were calculated from the same machining trials and compared with the surface roughness. This time, however, the data from the last machining layer and the roughness measured after the completed machining were used.

In contrast to the measurement investigated in Sec. 3.2, the surface roughness now depends on both the initial surface condition and the machining parameters. Thorough inspections of the resulting surface roughness as a function of the initial condition and the processing parameters have shown that the original condition in fact represents the main influence. Following the analysis results described in the previous section, it is to be expected that the differentiation between the markedly rough and smooth resulting surfaces based on the data of the last machining layer is possible. This expectation was indeed confirmed by the analogous analyses of the last machining layers.

The next step was the investigation of the possibility to detect changes in the roughness induced by the USP processing. For this, only the surfaces with the same initial state were compared among each other. In Fig. 3, an example of the direct comparison of data collected during the first and the last layer on two specimens polished with $S_a = 0.025\ \mu$m over the resulting roughness is given.

Here, each of the 99 processing parameters is represented by the total fluence, which considers the pulse overlap of two consecutive bursts assuming a pulse overlap of 1 within a burst:[36]

$$F_{\text{tot}} = \frac{\text{PPB} \cdot F_0 f_{\text{REP}} \cdot w_0}{v_{\text{scan}}}, \tag{2}$$

where f_{REP} is the repetition frequency, w_0 is the laser spot radius, and v_{scan} is the scan speed. This procedure was repeated on different specimen pairs, with the same result: All the analyzed characteristics of the secondary emissions are more dependent on the machining parameters than on the condition of the surface. It can therefore be concluded that it is not possible to investigate the

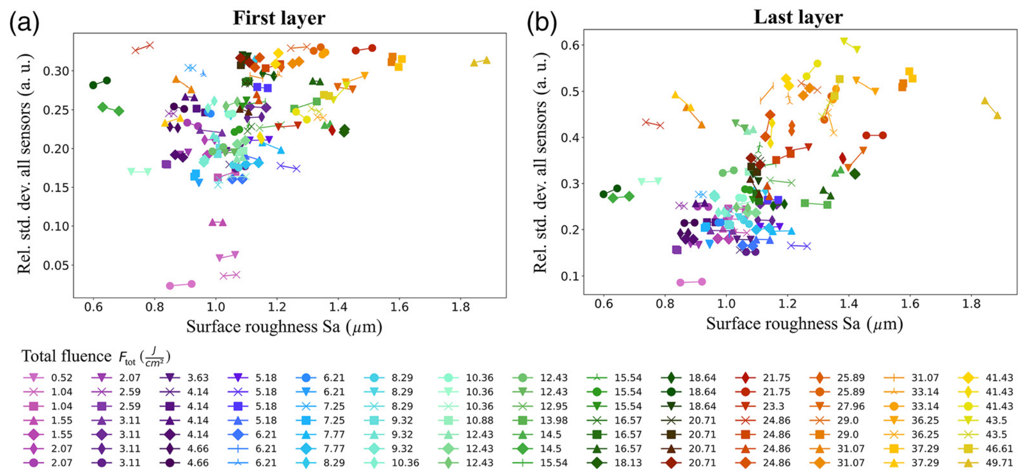

Fig. 3 Multiplied relative standard deviations of all signals within (a) the first and (b) last layer in dependence of the resulting roughness for two specimens with initial surface roughness $S_a = 0.025\ \mu$m and total fluences [J/cm^2].

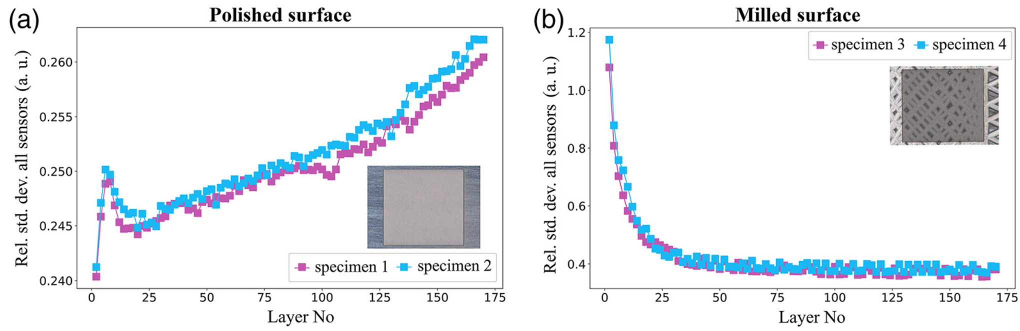

Fig. 4 Relative standard deviation of optical emissions within each layer over the number of layers for two sets of initial surfaces: (a) a polished surface and (b) a milled surface.

Table 1 Surface roughness of specimens from Fig. 4.

Specimen label	1 (μm)	2 (μm)	3 (μm)	4 (μm)
Initial Sa	0.025	0.025	12	12
Resulting Sa	1.00	1.06	6.25	6.72

resulting roughness based solely on the relative standard deviations of signals acquired while processing the last layer.

In the final step, the same characteristic was determined for each layer individually. The goal of this analysis is to explore the possibilities for monitoring relative changes during the machining. Examples of two groups of initial surfaces treated with PPB = 1 and $F_0 = 4.14\ \mathrm{J/cm^2}$ are shown in Fig. 4. To eliminate the dependency on the scan direction, this illustration only considers every other machining layer. Both the increase in surface roughness for the polished surfaces and its decrease for the milled ones are reflected in the relative standard deviation of the optical emissions.

Table 1 gives an overview of the surface roughness before and after machining for the four specimens from Fig. 4.

Generally, it can be concluded that the method described here is not sufficient for the detection of the subtle differences between the absolute values of the surface roughness. However, the change in surface condition during machining can be tracked through the changes in relative standard deviation. This result is used as a basis for implementing the analysis for the defect detection and localization.

4 Localization of Defects

4.1 *Experiment Design for Online Defect Detection*

To accelerate the initial development of an automatic defect detection, a demonstrative parameter set was chosen that provokes holes on a workpiece surface after only a few machined layers. Therefore, the sample structure from Fig. 5 was processed with pulse overlap of 96%, feed rate of 0.5 m/s, PPB = 1 and a fluence of $2.5\ \mathrm{J/cm^2}$.

Figure 6 shows 2D false-color representations of the intensities of all optical emissions acquired during the machining of both 5th and 15th layer. A qualitative comparison with the microscopic images from Fig. 5 already confirms the plausibility of the defect detection from the recorded emissions.

Moreover, the data depicted in Fig. 6 reveal how each recorded wavelength range adds an additional aspect to the knowledge about the surface state. While the point-shaped defects are most clearly distinguishable from their surroundings in the raw data of the recorded laser reflection, the line-shaped anomalies are more vividly visible in the images of both IR- and VIS-

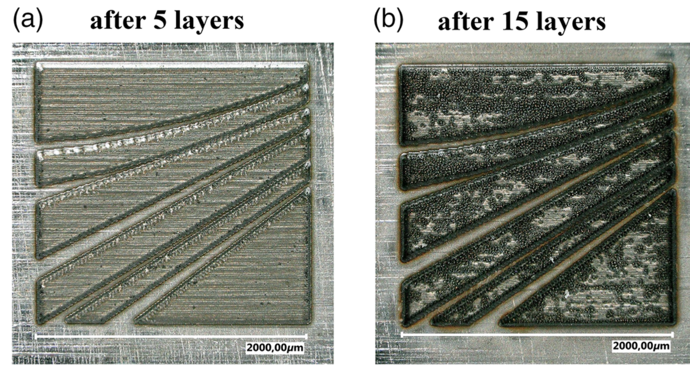

Fig. 5 Microscopic images of the sample structure (a) defect-free, after five layers; and (b) defect-containing, after 15 layers.

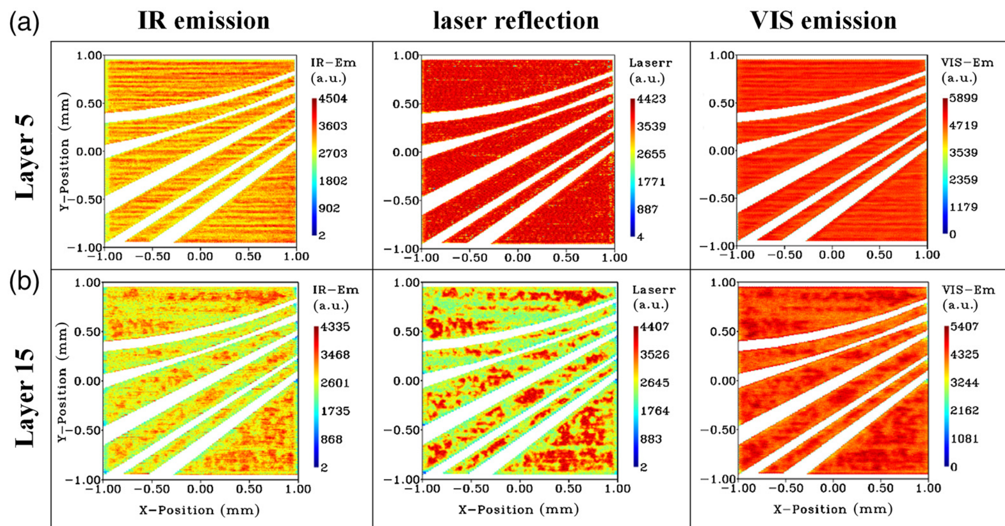

Fig. 6 2D representation of the raw data during the machining of the structure from Fig. 5. (a) During the fifth layer and (b) during the 15th layer for each of the three sensors indicated by the column name.

emissions. These horizontal lines originate from the surface topography prior to laser structuring, which can be seen around the sample structures in Fig. 5. Therefore, other than the point-like defects, they are already visible in the emission data of the first few layers, as shown in Fig. 6 and are highly dependent on the choice of the scan direction.

4.2 *Data Analysis for Offline Defect Detection*

From the beginning of this analysis, the future objective of implementing an online detection and feedback was considered. One of the main requirements for this is the sequential analysis able to run in parallel with the data acquisition. Furthermore, due to the limited memory capacity of the FPGA board, only as short as possible time series should be processed at any given moment. Another important goal was the development of a universal error detection, which can be transferred to machining with other processing parameters and different machines. The evident error detection based solely on emission intensities that follows from Fig. 6 is insufficient, because it is dependent on the absolute values of the process emissions and thus is not generally applicable.

In the first step, the defect detection was analyzed using the complete time series data of one processing layer. All analyses were performed on the one-dimensional data of each emission type and the results were subsequently mapped to a 2D plane for verification. Figure 7 shows

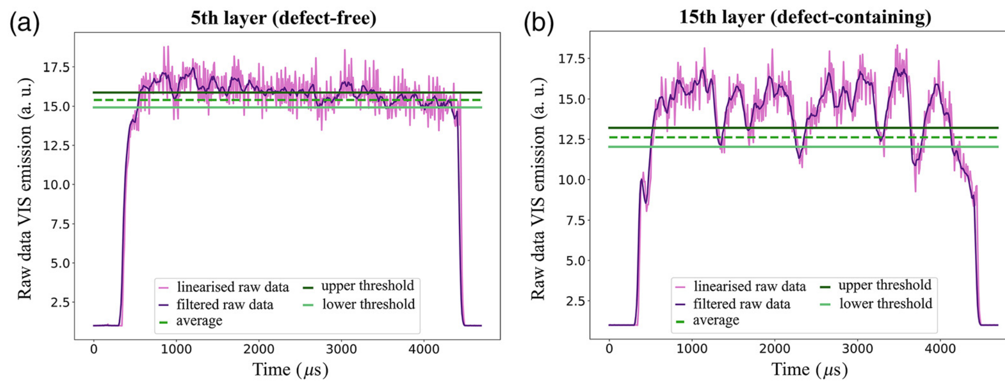

Fig. 7 Demonstration of the analysis procedure on an example of VIS-emission raw data during a single scan line for (a) one defect-free and (b) one defect-containing layer; here, the thresholds are symmetrically calculated by computing $I_{\text{filtered}} \pm 0.025 \cdot \text{mean}(I_{\text{filtered}}) \cdot \text{std}(I_{\text{filtered}})$ within one layer.

the analysis procedure on an example of VIS emissions for a defect-free and a defect-containing layer.

For each pair of coordinates, an individual calculation was performed to determine whether the corresponding optical emissions indicate a surface defect. To achieve this, the deviation of every data point from the signal's mean value was observed. The mean was calculated from the entire layer, but the laser-off areas as well as 80 data points after the rising and before the falling edge of the laser modulation signal were omitted. To differentiate between the deviations that indicate a defect and the ones originating from the noise, a tolerance band was defined, within which no decision can be made. The limits of this tolerance band are calculated for each layer separately. For its determination, the standard deviation of the emission intensities within that layer was taken into account. Moreover, the VIS emissions were low-pass prefiltered by forming a moving average with five datapoints since they contain high-frequency disturbances that do not originate from the machining.

In contrast to a detection based on absolute values that follow from Fig. 6, this method is transferrable to a broader range of use cases. The comparison with the mean value contributes to the independence of the processing parameters. The tolerance band limits that depend on the standard deviation within one layer, enable the detection of defects regardless of how pronounced they are.

The results of this analysis are presented in Fig. 8. For all three emission signals, the defects are manifested by a decrease in signal levels and are highlighted in red. This behavior can be explained by a local rise of the surface roughness. In these areas, the diffuse reflection increases, whereas the directional reflection decreases. This can lead to less light deflection toward the detectors, resulting in negative deviations from the mean value of the optical process emissions.

In the next step, the analysis was further improved to achieve a data reduction as well as rapid response times during the future closed loop control. Instead of the data of one entire layer, it now executes on time series collected within a 1-ms long rolling window. At the constant sampling rate of 100 kHz used in this case, this window length corresponds to a set of 100 data points. The results of the analysis performed on the time series before being mapped on a 2D plane are depicted in Fig. 9.

To achieve these results, two further adjustments had to be made compared to the analysis within the whole layer. First, the areas close to the laser modulation signal edges are not omitted. This is not required anymore, because the local calculation of the tolerance limits insures more stringent criteria for the differentiation between defects and noise that originates from the signal edges. In addition, the factors for calculating the tolerance limits had to be correspondingly adjusted.

Although the results from Fig. 9 show successful detection of most defects, this approach is not free from disadvantages. For example, the line-shaped defects that spread parallelly to the scan direction are not visible if their size exceeds the window length. Moreover, even the point-shaped defects are detectable up to a maximum size, which is also determined by the window

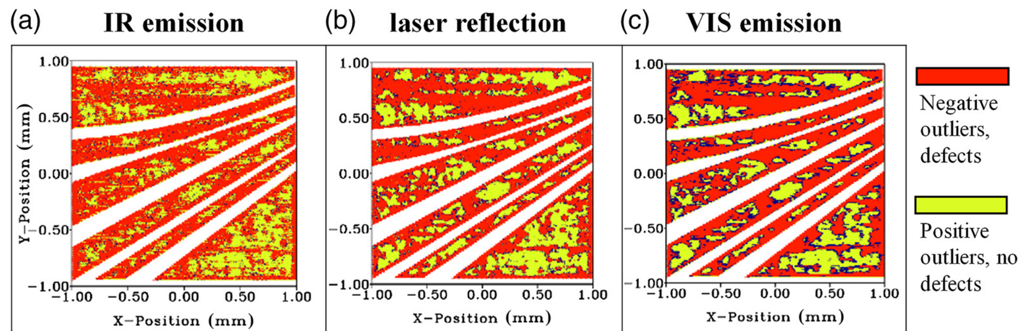

Fig. 8 2D representation of the analyzed raw data of the defect-containing layer for each of the detectors: [(a)–(c) IR-emission, laser reflection, and VIS-emission]. The outliers are classified by checking whether the filtered data cross the upper and lower thresholds from Fig. 7.

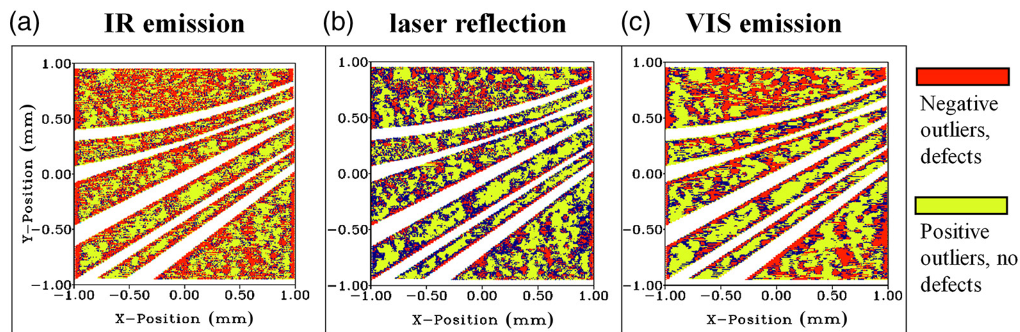

Fig. 9 Analyzed data of the defect-containing layer for each of the detectors [(a)–(c) IR-emission, laser reflection, and VIS-emission]. The outliers are classified by checking whether the filtered data cross the thresholds determined according to Fig. 7; instead of computing the thresholds within a whole layer, here, they are calculated in a 1-ms-long rolling window.

length. Beside the size of the defects, the scanning speed imposes another limitation to the detection for further applications. This is because the spatial resolution is directly dependent on the scanning speed due to the constant data acquisition rate.

4.3 *Automation of the Defect Detection*

The aim of this analysis step was to define a factor that describes the extent of defects and can be used as a criterion for terminating the machining. Similar to the previous section, a sequential analysis on a small sample plays an essential role here as well. This is because the processing is to be interrupted as quickly as possible after the extent of errors has exceeded a predefined limit.

As the starting point, the results of the analysis within a rolling window were used. In this case, simply counting the negative outliers would be insufficient since they are present even in the data that correspond to the defect-free surfaces. However, it is evident that they become increasingly organized into larger clusters as actual defects appear on the workpiece surface. From this observation, a factor was derived that is proportional to both the number and the area of the red regions from Fig. 9.

In order to calculate this measure of defects directly from the one-dimensional data, the number of negative outliers within a 10-datapoint long rolling window is sought. The derived measure corresponds to the total number of such windows that contain at least nine negative outliers. This factor was calculated for each of the 15 layers during the structuring of the geometries from Fig. 5. In Fig. 10, it is plotted over the layer's number. The figure depicts both the factors determined from the individual sensor signals as well as the overall measure derived from their multiplication.

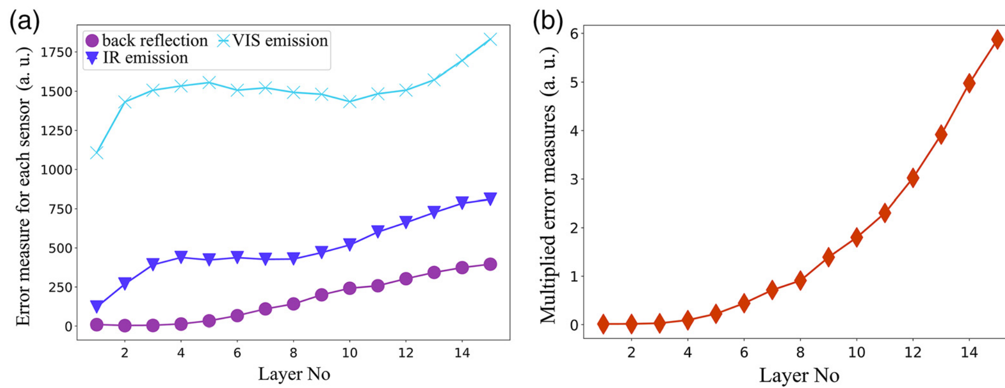

Fig. 10 Automatically determined error measures over the ordinal number of the structured layer. They represent the number of adjacent negative outliers from Fig. 9 inside a 10-datapoint rolling window along the scan direction. (a) For each individual sensor and (b) multiplied and normalized error measures from the left graph.

The multiplied error measures from Fig. 10 right is a unitless quantity. To improve the clarity of the representation, its y-axis is divided by a constant factor. It increases with the increasing number of layers, which stands in agreement with the microscope images. On the other hand, the factor derived from the VIS emissions shows a decrease between the layers 5 and 10. Therefore, omitting the VIS emissions would in this case improve the accuracy of the detection. However, this would actually impair the accuracy for the last four layers of the same structure. There, the differentiation based on the analysis results of VIS emissions is even finer than based on both other emissions.

The error measure is proportional to the number and the area of the red areas from Fig. 9. From both Figs. 9 and 10, it follows that the VIS-photodiode is most sensitive to this kind of disturbances. However, due to calculating the overall error measure as a multiplication of all, the absolute value of each of them does not play a role.

A possible improvement of the algorithm that follows this would be to introduce weighting factors for the individual sensors. They must be previously determined depending on the significance of the corresponding data and the superimposed noise. Furthermore, an additional analysis perpendicular to the scan direction would allow the detection of defects that spread along the second axis.

4.4 *Implementation of the Online Analysis*

Using the results of the offline analyses, the FPGA-based data acquisition system, described in Sec. 2.2, was extended to detect the defects in parallel to the machining process. The analysis algorithm had to be adjusted to better fit the online analysis requirements. For example, instead of a rolling window for the calculation of the mean value and the extraction of deviations, a sliding 1-ms long window was used. In contrast to the case of offline analysis, this has no negative effect on the speed of the online evaluation. The sliding window analysis even has an important advantage. For each data point, the change in emission intensities at the rising edge of the laser modulation is automatically considered separately and is therefore more accurate. Moreover, to omit the areas where the laser was idle, its modulation signals are monitored continuously and processed by the same controller.

Another adjustment in comparison to the analysis from Sec. 4.2 is the linearization of the raw data, which was excluded in this implementation. To compensate for the altered conditions, the threshold values for the outlier detection were redetermined. Nevertheless, they are still calculated relative to the mean value and as a function of the standard deviation within 1 ms.

To implement the feedback directed to the user, a threshold was introduced, above which the determined number of defects is considered unacceptable. The calculation of this threshold occurs automatically and is based on the number of defects extracted during the processing of the first layer. It is therefore reset at the beginning of the machining of a new structure.

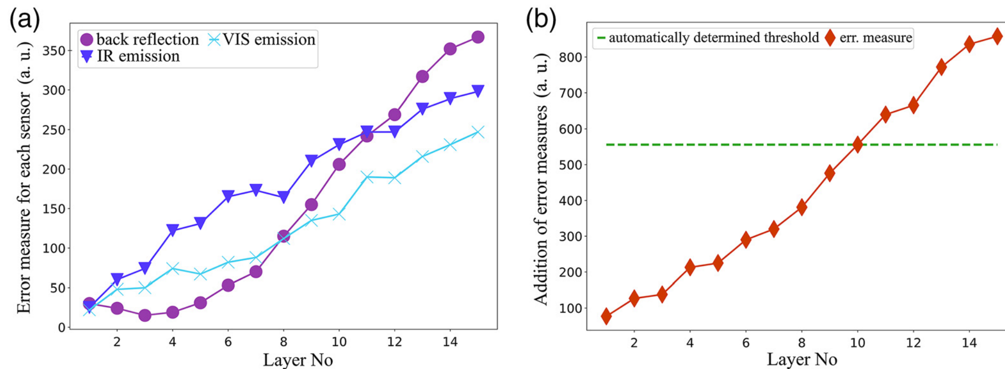

Fig. 11 Automatically determined error measures over the ordinal number of the structured layer, (a) for each individual detector and (b) addition of the error measures from the left graph. Here, the termination threshold is the first value that exceeds the five times error measure computed from the data collected during the first layer.

Once the threshold is reached during the processing, a message is forwarded to the PC. In the case of processing with an unchanged parameter set, this is assumed to be an irreversible state. Therefore, this message is only reset at the beginning of the processing of a new structure or when a parameter change is made.

Following its implementation in the FPGA, the error detection and feedback were validated using the set of parameters from Sec. 4.1 and both the sample structure from Fig. 5 as well as a rectangular area. The processing was performed on a polished surface with two different orientations of the scan direction relative to the surface texture induced by the preprocessing. As a result, the error message was generated without an exception. However, the moment of its generation was dependent on both the structured geometry and its orientation relative to the initial state of the surface.

To investigate the intermediate results more closely, the FPGA design was temporarily modified so that it forwards the internally determined factors to the PC. An example of the error measures extracted parallelly to the processing are given in Fig. 11. The horizontal line denotes the automatic ally determined termination criterion, i.e., the moment at which the error message was generated. In contrast to the offline analysis, the characteristic of the general error measure is linear due to its calculation by adding instead of multiplying the individual factors.

Based on these results, the extension of the monitoring system to terminate the machining immediately after the defect detection is realizable by modulating one of its digital outputs. Long-term developments include an automatic triggering of one or more additional intermediate processing steps in order to flatten the defects, e.g., by means of the already investigated USP-laser polishing.[37] Further specific strategies to automatically control the processing parameters in order to remove or prevent the defect emergence are equally possible.

5 Conclusion and Outlook

The aim of the present work was the data analysis and algorithm development for the extension of a system for monitoring of surface properties during the USP laser structuring. Long-term objectives of this development include enabling an automated parameter adjustment in response to the surface roughness measured during the processing. This would significantly accelerate the parameters studies, thereby decreasing the duration of the time-consuming process development immensely. Moreover, the detection of the emerging defects in parallel to the machining is an essential step for achieving the first-time-right manufacturing. Both objectives are realizable only with a highly reliable monitoring system, able to analyze the surface condition in real time. Additionally, the monitoring system should not interfere with the machining.

In the scope of this work, a monitoring system that satisfies the conditions was thoroughly inspected. It is based on a simultaneous collection of various secondary process emissions and the scanner position, enabling both a high temporal and spatial resolution. It was evaluated for

three different application areas: detection of the initial surface state, monitoring of the changes during the processing, and online defect detection. Successful results were achieved for the differentiation of pronouncedly rough and smooth surfaces during the machining with in advance known parameters. This is possible through comparatively simple data analysis such as the calculation of the relative standard deviation of optical emissions within one processing layer. The method furthermore proved suitable for the tracking of changes in surface condition during the machining. In addition, following the initial offline evaluation of optical emission data, the defect localization was implemented as a real-time analysis executed in the FPGA used for the data acquisition. By forwarding the analysis result to the user interface, the system is able to successfully inform the user about the defect formation in parallel to the processing.

In contrast to the previous investigations that describe the detection of fluctuations caused by the processing (e.g., parameter changes), the innovations presented in this work lie in the analysis of correlations between the process emissions and the state of the surface. Furthermore, a data analysis parallel to the processing was demonstrated, which generates a decision for each data point at a rate of 100 kHz. The system can be programmed flexibly and thus expanded to include real-time data analyses for further applications as well as for process control.

However, there is still room for improvements. For example, the system can be extended to record additional information as well as execute more advanced analyses, e.g., the data-based approaches. Nevertheless, the results described in this work show a great potential for both reliable defect detection and surface roughness monitoring in parallel to the machining as well as the closed-loop control.

Acknowledgments

This work has received funding from the European Union's Horizon 2020 research and innovation programme under Grant Agreement No. 825201. It is based on a publication in a SPIE proceedings, Paper No. 11989-36. The authors declare that there is no conflict of interest.

References

1. T. Nicolay and V. Bayer, "Den Schweißpunkt immer im Fokus," *Laser Technik J.* **6** 33–35 (2009).
2. T. Bautze and A. Zösch, "Laserschweißen mit höchster Qualität bei reduzierter Leistung," *Laser Technik J.* **8**(6), 29–33 (2011).
3. I. Smurov, "Pyrometry applications in laser machining," *Proc. SPIE* **4157**, 55–66 (2001).
4. M. Müller, *Prozessüberwachung beim Laserstrahlschweißen durch Auswertung der reflektierten Leistung*, Herbert Utz Verlag, München (2002).
5. M. Bastuck et al., "AkuProLas: acoustic inline process monitoring for laser welding applications," in *19th World Conf. Non-Destructive Testing* (2016).
6. C. Knaak et al., "Machine learning as a comparative tool to determine the relevance of signal features in laser welling," *Proc. CIRP* **74**, 623–627 (2018).
7. D. Schindhelm, "In-Prozess Qualitätssicherung für das Laserstrahlschneiden von Metallen," Laser in der Materialbearbeitung Forschungsberichte des IFSW (2013).
8. J. de Keuster, J. R. Duflou, and J.-P. Kruth, "Monitoring of high-power CO_2 laser cutting by means of an acoustic microphone and photodiodes," *Int. J. Adv. Manuf. Technol.* **35**(1–2), 115–126 (2007).
9. Y.-M. Lai and N.-H. Cheung, "Pulsed laser-induced damage threshold studies of thin aluminum films on quartz: simultaneous monitoring of optical and acoustic signals," *Rev. Sci. Instrum.* **64**(6), 1606–1610 (1993).
10. A. Ortiz and J. Schneiter, "Method and apparatus for optically/acoustically monitoring laser materials processing" (1990).
11. T. Purtonen, A. Kalliosaari, and A. Salminen, "Monitoring and adaptive control of laser processes," *Phys. Proc.* **56**, 1218–1231 (2014).
12. M. Honer, *Prozesssicherungsmassnahmen beim Bohren metallischer Werkstoffe mittels Laserstrahlung*, Herbert Utz Verlag, München (2004).

13. D. Walter, "Online-Qualitätssicherung beim Bohren mittels ultrakurz gepulster Laserstrahlung," Laser in der Materialbearbeitung Forschungsberichte des IFSW (2010).
14. F. Mezzapesa et al., "High-resolution monitoring of the hole depth during ultrafast laser ablation drilling by diode laser self-mixing interferometry," *Opt. Lett.* **36**(6), 822–824 (2011).
15. M. Stafe, C. Negutu, and I. M. Popescu, "Real-time determination and control of the laser-drilled holes depth," *Shock Waves* **14**(1–2), 123–126 (2005).
16. J. Shin and J. Mazumder, "Plasma diagnostics using optical emission spectroscopy in laser drilling process," *J. Laser Appl.* **28**(2), 22008 (2016).
17. R. Petkovšek et al., "Optodynamic monitoring of laser micro-drilling of glass by using a laser probe," *Appl. Phys. A* **93**(1), 141–145 (2008).
18. P. Weber, *Steigerung der Prozesswiederholbarkeit mittels Analyse akustischer Emissionen bei der Mikrolaserablation mit UV-Pikosekundenlasern*, Karlsruher Institut für Technologie (KIT) (2014).
19. S. Conesa, S. Palanco, and J. J. Laserna, "Acoustic and optical emission during laser-induced plasma formation," *Spectrochim. Acta B: Atomic Spectrosc.* **59**(9), 1395–1401 (2004).
20. H. Chae and S. Min Parka, "Microphone detection of laser ablation," *Rev. Sci. Instrum.* **68**(12), 4627–4628 (1997).
21. T. Efthimiopoulos et al., "Laser ablation rate of materials using the generated acoustic waves," *J. Phys. D: Appl. Phys.* **31**(19), 2648–2652 (1998).
22. F. Mitsugi et al., "Observation of phenomena after pulsed laser irradiation of solid with optical wave microphone," *Japanese J. Appl. Phys.* **51**(1S), 01AC10 (2012).
23. F. Mitsugi et al., "Optical wave microphone measurements of laser ablation of copper in supercritical carbon dioxide," *Thin Solid Films* **547**, 81–85 (2013).
24. E. V. Bordatchev and S. K. Nikumb, "Effect of focus position on informational properties of acoustic emission generated by laser–material interactions," *Appl. Surf. Sci.* **253**(3), 1122–1129 (2006).
25. C. Gehrke, *Überwachung der Struktureigenschaften beim Oberflächenstrukturieren mit ultrakurzen Laserpulsen*, Herbert Utz Verlag, München (2013).
26. Y. Whan Park and S. Rhee, "Study of a line width estimation model for laser micro material processing using a photodiode," *Opt. Laser Technol.* **39**(7), 1461–1471 (2007).
27. P. Strohm et al., "Controlling laser material processing with real-time algorithms on cellular neural networks," in *SENSOR+TEST Conf. OPTO Proc.* (2011).
28. R. Kunze, G. Mallmann, and R. Schmitt, "Inline plasma analysis as tool for process monitoring in laser micro machining for multi-layer materials," *Phys. Proc.* **83**, 1329–1338 (2016).
29. D. Diego-Vallejo et al., "Selective ablation of Copper–Indium–Diselenide solar cells monitored by laser-induced breakdown spectroscopy and classification methods," *Spectrochim. Acta B: Atomic Spectrosc.* **87**, 92–99 (2013).
30. V. P. Bessmeltsev, E. D. Bulushev, and N. V. Goloshevsky, "Adaptive control system for laser micromachining devices," *Proc. SPIE* **7996**, 79960C (2011).
31. M. Wiesner et al., "Optical coherence tomography for process control of laser micromachining," *Rev. Sci. Instrum.* **81**(3), 33705 (2010).
32. R. Schmitt and G. Mallmann, "Process monitoring in laser micro machining," *Photonik Int.* **11**(3), 57–59 (2013).
33. R. Schmitt et al., "Automated process initialization of laser surface structuring processes by inline process metrology," *Phys. Proc.* **41**, 887–895 (2013).
34. M. Paulo Raele et al., "Focus tracking system for femtosecond laser machining using low coherence interferometry," *Sci. Rep.* **9**, 4167 (2019).
35. M. Zuric, "Multi-sensor system for real-time monitoring of laser micro-structuring," *J. Laser Micro/Nanoeng.* **3**(14), 245–254 (2019).
36. A. Brenner, "Sequentielle Ultrakurzpuls-Laserbearbeitung zur effizienten Oberflächentexturierung" (2021).
37. A. Brenner et al., "Laser polishing using ultrashort pulse laser," *Proc. SPIE* **11268**, 112680P (2020).

Milena Zuric received her bachelor's degree in electrical engineering from the RWTH Aachen University in 2014 followed by a master's degree 2 years later, specializing in the field of micro- and nanoelectronics. During her studies and internships, she obtained practical experience in embedded systems programming. She currently combines this knowledge with laser-based manufacturing while working on her PhD at the Fraunhofer Institute for Laser Technology, where she focuses on real-time monitoring and control of laser microstructuring.

Andreas Brenner is the leader of team Thin Film Surface Structuring at Fraunhofer Institute for Laser Technology. After completing his bachelor's studies in mechanical engineering, he received a master's degree from the RWTH Aachen University in 2015, followed by a PhD in 2020. His field of research includes process development to increase the productivity of ultra-short pulse laser structuring.